PNAS RESEARCH ARTICLE | EARTH, ATMOSPHERIC, AND PLANETARY SCIENCES

Sea-surface temperature pattern effects have slowed global warming and biased warming-based constraints on climate sensitivity

Kyle C. Armour[a,b,1,2], Cristian Proistosescu[c,d,1], Yue Dong[e], Lily C. Hahn[f], Edward Blanchard-Wrigglesworth[a], Andrew G. Pauling[g], Robert C. Jnglin Wills[a,h], Timothy Andrews[i], Malte F. Stuecker[j], Stephen Po-Chedley[k], Ivan Mitevski[l], Piers M. Forster[m], and Jonathan M. Gregory[j,n]

Edited by Isaac Held, Princeton University, Princeton, NJ; received July 17, 2023; accepted December 15, 2023

The observed rate of global warming since the 1970s has been proposed as a strong constraint on equilibrium climate sensitivity (ECS) and transient climate response (TCR)—key metrics of the global climate response to greenhouse-gas forcing. Using CMIP5/6 models, we show that the inter-model relationship between warming and these climate sensitivity metrics (the basis for the constraint) arises from a similarity in transient and equilibrium warming patterns within the models, producing an effective climate sensitivity (EffCS) governing recent warming that is comparable to the value of ECS governing long-term warming under CO_2 forcing. However, CMIP5/6 historical simulations do not reproduce observed warming patterns. When driven by observed patterns, even high ECS models produce low EffCS values consistent with the observed global warming rate. The inability of CMIP5/6 models to reproduce observed warming patterns thus results in a bias in the modeled relationship between recent global warming and climate sensitivity. Correcting for this bias means that observed warming is consistent with wide ranges of ECS and TCR extending to higher values than previously recognized. These findings are corroborated by energy balance model simulations and coupled model (CESM1-CAM5) simulations that better replicate observed patterns via tropospheric wind nudging or Antarctic meltwater fluxes. Because CMIP5/6 models fail to simulate observed warming patterns, proposed warming-based constraints on ECS, TCR, and projected global warming are biased low. The results reinforce recent findings that the unique pattern of observed warming has slowed global-mean warming over recent decades and that how the pattern will evolve in the future represents a major source of uncertainty in climate projections.

climate sensitivity | global warming | climate dynamics

Significance

Climate models show a tight relationship between post-1970s global warming and climate sensitivity. The latest IPCC Assessment Report used observations of the warming rate to constrain Earth's climate sensitivity and warming projections. However, climate models do not reproduce the observed spatial pattern of warming, introducing a bias in the modeled warming-sensitivity relationship that results in overly-confident constraints. The findings suggest that observed warming over recent decades provides very little information about climate sensitivity, and that constraints on high-sensitivity values must come from other lines of evidence. Additionally, projections of global warming need to account for how the spatial pattern will evolve in the future. Since climate models fail to reproduce recent patterns, this introduces a major uncertainty in climate projections.

Equilibrium climate sensitivity (ECS) and transient climate response (TCR) are key metrics of the global-mean surface temperature response to increasing greenhouse-gas concentrations. They represent the warming under a doubling of atmospheric carbon dioxide (CO_2) at equilibrium and at the time of CO_2 doubling, respectively. Model values of ECS and TCR are strongly correlated with projections of 21st century warming (1, 2). The recent IPCC Sixth Assessment Report (AR6) assessed the ranges of ECS and TCR to be substantially more narrow than in previous Reports (2) following advances in scientific understanding of several independent lines of observational evidence (e.g., ref. 3). Narrower ranges of ECS and TCR in turn translate to better-constrained projections of 21st century warming compared to projections based on global climate models (GCMs), which span wider ECS and TCR ranges (4).

One major update in IPCC AR6 was a reinterpretation of historical energy budget constraints on climate sensitivity based on observed warming since the 1800s. While the historical energy budget was once thought to place strong constraints on ECS (5–7), in IPCC AR6 it was assessed to provide relatively weak constraints, particularly at the high end of the climate sensitivity range. This assessment was based on i) stubbornly large uncertainty in the radiative forcing that drove historical warming, owing primarily to uncertainty in aerosol forcing, and ii) work since AR5 showing that differences between historical and future (centennial timescale) sea-surface temperature (SST) trend patterns result in estimates of ECS that are biased low (2, 3, 8–19). This SST pattern effect occurs because the feedbacks governing Earth's global radiative response per degree of global warming depend on the spatial pattern of that warming. In particular, warming since the 1800s has been relatively slow within key regions of positive (destabilizing) radiative feedbacks including the eastern tropical Pacific Ocean and Southern Ocean; in the long term, however, these regions are expected to warm more than the global mean, leading

The authors declare no competing interest.

This article is a PNAS Direct Submission.

[1]K.C.A. and C.P. contributed equally to this work.

[2]To whom correspondence may be addressed. Email: karmour@uw.edu.

This article contains supporting information online at https://www.pnas.org/lookup/suppl/doi:10.1073/pnas.2312093121/-/DCSupplemental.

Published March 11, 2024.

to a less-negative global feedback and thus an increase in the climate's sensitivity to greenhouse-gas forcing (8, 9, 19–27). Thus, the value of the effective climate sensitivity (EffCS) governing historical warming is thought to be lower than the value of ECS governing equilibrium warming under CO_2 forcing (2, 3).

Another major advance in recent years has been the development of novel observational constraints (often referred to as "emergent constraints"), wherein coupled GCMs are used to find a correlation between an observable quantity and something we wish to predict, and then the model-based relationship is combined with observations of that quantity to derive constrained predictions (28–31). Strong constraints on ECS and TCR have been derived using the post-1970s rate of global-mean warming (18, 32–34): Because GCMs with higher ECS and TCR values tend to overestimate the observed rate of warming, the implication is that high values of climate sensitivity are less likely. This constraint was proposed to avoid the issues plaguing energy budget constraints based on warming since the 1800s (32): Because global aerosol radiative forcing changes have been relatively small since the 1970s, the use of this period substantially reduces the impact of uncertainty in radiative forcing; and SST pattern effects are implicitly accounted for in the use of GCMs to derive the correlation between recent warming and ECS (or TCR).

As summarized in Forster et al. (2), studies using post-1970s global warming as an observational constraint produce narrow bounds on ECS (with best estimates of 2.6 to 2.8 °C and 5 to 95% ranges within 1.5 to 4.1 °C) and TCR (with best estimates of 1.6 to 1.7 °C and 5 to 95% ranges within 1.0 to 2.3 °C). Collectively, these studies provided the strongest constraints on ECS and TCR of any of the main lines of evidence assessed in IPCC AR6 and were a primary justification for assessing the upper bounds on the ECS *likely* (2.5 to 4 °C) and *very likely* (2 to 5 °C) ranges to be lower than in previous Reports. These narrower ranges also suggest that GCMs with ECS values higher than about 5 °C, of which there are many (35) in the Coupled Model Intercomparison Project phase 6 (CMIP6, ref. 36), may be less valid for projecting future warming (e.g., refs. 2 and 37).

For such a constraint to be robust, it must exhibit two key properties. First, because many spurious correlations between observable and predicted quantities of interest can be found by chance within GCMs (38), any correlation that is used as the basis for the constraint must rest on sound physical principles (28, 29, 31, 39). Second, the GCMs used as the basis for the constraint must not share a common bias, relative to nature, in their representation of this correlation (e.g., refs. 28 and 40).

For constraints on ECS and TCR based on observed post-1970s global warming, there is a strong physical basis for the modeled correlation: Higher ECS and TCR correspond to a less-efficient radiative response per degree of global warming which, all else being equal, should lead to a faster rate of global warming under greenhouse-gas forcing. And the constraints have been shown to produce similar results whether using CMIP5 or CMIP6 models (18, 32–34), providing confidence in their robustness.

However, recent work has found that historical simulations of CMIP5/6 models generally fail to simulate the observed spatial pattern of post-1970s SST trends (16, 17, 41, 42). In particular, the models produce relatively weak spatial gradients in SST trends, with somewhat enhanced warming in the eastern tropical Pacific Ocean and at high latitudes, while observations show strong spatial gradients in SST trends, with cooling in the eastern Pacific and Southern Oceans.

These model-versus-observed discrepancies in SST trend patterns influence the radiative feedbacks that govern climate sensitivity: When atmosphere GCMs are forced with the observed post-1970s SST trends, they generally produce global radiative feedbacks that are substantially more negative (lower EffCS) than feedbacks produced over this period by historical simulations of the same coupled GCMs (16, 17). This suggests that there is in fact a common bias across CMIP5/6 GCMs that could affect the modeled relationship between post-1970s warming and climate sensitivity metrics. It is possible, for instance, that GCMs overestimate recent warming in part due to their biases in simulated warming patterns, with relatively too much warming in key positive feedback regions, rather than simply having too-high values of ECS or TCR (as is assumed by the observational constraint). IPCC AR6 noted this possibility, finding it *more likely than not* that constraints on ECS and TCR based on observed post-1970s global warming are biased low (2); but without studies quantifying the magnitude of this bias, no corrections could be made.

Here we evaluate the potential for SST pattern effects to bias observational constraints on ECS and TCR via their influence on the CMIP5/6-based relationship between post-1970s global warming and these climate sensitivity metrics. We first reproduce constraints on ECS and TCR based on recent warming and find similar results to the published literature. We then analyze a subset of CMIP5/6 models that provide the output necessary to accurately calculate radiative feedbacks (and corresponding EffCS) over the historical period. We find that CMIP5/6 models warm too much over recent decades in large part due to their failure to replicate the observed post-1970s SST trend patterns, and thus even high values of climate sensitivity are consistent with the observed global warming rate. We conclude that the proposed constraints on ECS and TCR based on recent global warming are biased low. We evaluate the robustness of our findings using energy-balance model simulations and coupled-model (CESM1-CAM5) simulations that better replicate observed patterns via tropospheric wind nudging or Antarctic meltwater fluxes. Finally, we discuss implications of these results for recent climate sensitivity assessments and for 21st century warming.

The Relationship between Post-1970s Warming and Climate Sensitivity

While several different time periods have been used to place observational constraints on climate sensitivity from recent global warming (32, 33), here we focus on 1981 to 2014 following Tokarska et al. (34). We show relationships between the rate of global-mean surface warming over this period and ECS (Fig. 1*A*) for all GCMs that provide the necessary output on the CMIP5/6 archives (21 CMIP5 models and 38 CMIP6 models; see *SI Appendix* for a list). While we focus on ECS in the main text, the full analysis using TCR produces similar results (*SI Appendix*). We calculate warming rates by averaging over all available ensemble members of each model's *historical* simulation (extended using RCP4.5 over years 2006 to 2014 for CMIP5 models), where each ensemble member is forced by identical historical greenhouse-gas, aerosol, volcanic, and solar forcings, and differ only in their phasing of internal variability. CMIP5/6 model values of ECS have been estimated using the standard approach of extrapolating to equilibrium the regression between global top-of-atmosphere energy imbalance and global temperature change over 150 y of abrupt CO_2 quadrupling simulations, scaled by a factor of a half to account for CO_2 doubling (35, 43, 44).

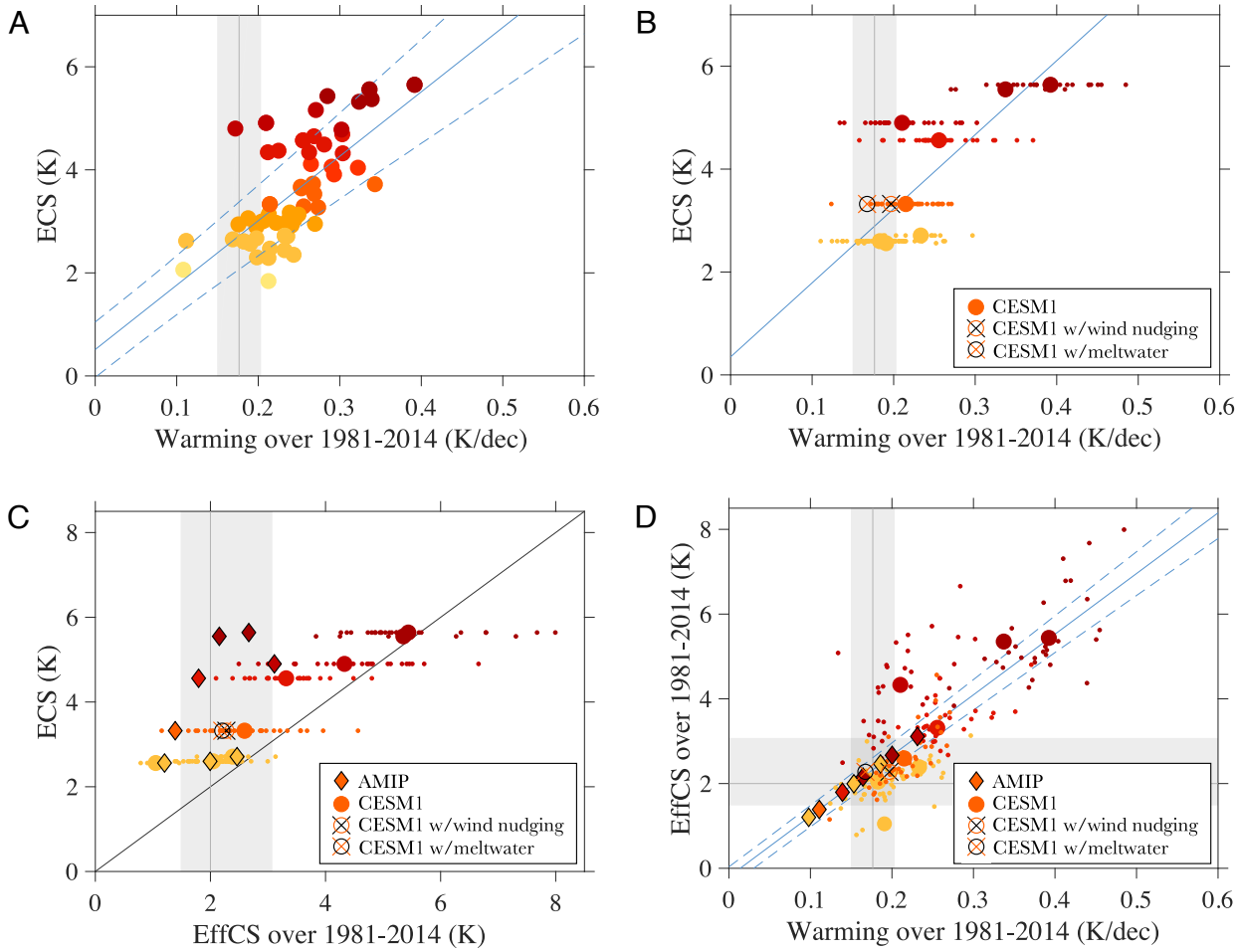

Fig. 1. Relationships between ECS, EffCS, and the 1981 to 2014 warming rate in CMIP5/6 models. (*A*) CMIP5/6 ECS versus warming rate using averages of all available ensemble members for each model (correlation $r = 0.68$); colors correspond to values of ECS. (*B*) Eight-model subset ECS versus warming rate with ensemble means shown as larger circles and ensemble members shown as smaller dots. (*C*) Eight-model subset ECS versus EffCS over 1981 to 2014 with ensemble means shown as larger circles and ensemble members shown as smaller dots; diamonds show EffCS values from AGCM simulations forced by observed SST and SIC trend patterns. (*D*) Eight-model subset EffCS over 1981 to 2014 versus warming rate with ensemble means shown as larger circles and ensemble members shown as smaller dots; diamonds show warming rates estimated based on EffCS values from AGCM simulations using the regression between EffCS and warming rate calculated from the eight-model subset (blue line). In *B–D*, open circles show CESM1-CAM5 simulations with wind nudging or meltwater fluxes as described in the text. Blue lines show fits calculated using ordinary least squares (OLS) regression, with dashed blue lines showing 5 to 95% ranges of fit parameters (*Materials and Methods*). Gray shading shows observational estimates (5 to 95% range) of observed warming rate (HadCRUT5, ref. 45) and EffCS (19). See *SI Appendix* for a list of models used.

We find a strong correlation between the 1981 to 2014 global warming rate and ECS (Fig. 1*A*) or TCR (*SI Appendix*, Fig. S1*A*). Using this regression (*Materials and Methods*), the observed warming rate of 0.18 °C dec^{-1} (0.15 to 0.21 °C dec^{-1}, 5 to 95% range) calculated from HadCRUT5 (45) gives ECS = 2.7 °C (1.5 to 3.9 °C) and TCR = 1.6 °C (1.1 to 2.1 °C), in good agreement with previous studies (18, 32–34).

To better understand the modeled relationship between global warming and climate sensitivity, we consider a subset of eight CMIP5/6 models representing all those that provide at least three *historical* ensemble members and the output necessary to accurately calculate radiative feedbacks over the historical period: CanESM5, CNRM-CM6-1, GISS-E2-1-G, HadGEM3-GC31-LL, IPSL-CM6A-LR, MIROC6, NorESM2-LM, and CESM1-CAM5. The relationships between 1981 and 2014 global warming rate and ECS are similar for this eight-model subset (Fig. 1*B*) to those found in the full CMIP5/6 ensemble (Fig. 1*A*). For each model, there is substantial spread in warming rates across ensemble members due to internal climate variability (Fig. 1*B*), raising two key questions: i) what factors control the variability in warming rates across model ensemble members? And, ii) do CMIP5/6 models accurately represent how those factors were expressed in observations over the period 1981 to 2014?

Each of the eight models in our subset has a corresponding CMIP6 *piClim-histall* simulation wherein the same atmospheric GCM (AGCM) was run with fixed pre-industrial SSTs and sea-ice concentrations (SICs) while all radiative forcing agents were varied as in the corresponding CMIP6 *historical* simulations. The *piClim-histall* simulations were performed as part of the Radiative Forcing Model Intercomparison Project (RFMIP, ref. 46) for CMIP6, while we perform our own *piClim-histall*-style simulation for CESM1-CAM5 following the same protocol. From these simulations, the historical effective radiative forcing (ERF) can be diagnosed from top-of-atmosphere radiation anomalies relative to pre-industrial conditions (17, 47), with a small correction for land warming (2, 48) (*Materials and Methods*). Using the standard model of global energy balance,

$$N = \lambda T + \mathrm{ERF}, \qquad [1]$$

where N is the global top-of-atmosphere radiation anomaly and T is the global near-surface air temperature anomaly (both relative to pre-industrial), we diagnose the global effective radiative feedback λ (<0 for a stable climate) from linear regression of $N - \mathrm{ERF}$ against T over the period 1981 to 2014 for each ensemble member (*Materials and Methods*). From this, we calculate EffCS for the period 1981 to 2014 as,

$$\mathrm{EffCS} = -\frac{\mathrm{ERF}_{2\times}}{\lambda}, \quad [2]$$

where $\mathrm{ERF}_{2\times}$ is the ERF from CO_2 doubling (35, 44) (*Materials and Methods*). EffCS is largely set by the value of λ both because it is in the denominator in Eq. **2** and because λ varies fractionally more than does $\mathrm{ERF}_{2\times}$ across models (35). EffCS can be interpreted as the equilibrium warming that would occur in response to CO_2 doubling if the value of λ calculated over the period 1981 to 2014 applied to that equilibrium state.

We find that there is a large spread in EffCS for the period 1981 to 2014 across ensemble members of each GCM (small dots in Fig. 1*C*). Moreover, differences in EffCS explain a large fraction of the variance ($r^2 = 0.61$) in the 1981 to 2014 warming rate across all ensemble members of our eight-model subset; those with EffCS values near 2 °C tend to produce warming rates in line with observations, while those with higher values of EffCS warm too much (Fig. 1*D*).

The high correlation between EffCS and the global warming rate can be understood by making the approximation $N = \kappa T$ in Eq. **1**, where κ is the ocean heat uptake efficiency representing all processes setting the amount of global ocean heat uptake per degree of global warming (e.g., refs. 49–51); a larger value of κ corresponds to a more efficient uptake of heat by the deep ocean and thus less surface warming. Then, the rate of warming can be approximated as (e.g., ref. 52),

$$\frac{dT}{dt} = \frac{d(\mathrm{ERF})/dt}{\kappa - \lambda}. \quad [3]$$

Calculating κ from regression of N against T over 1981 to 2014, and given $d(\mathrm{ERF})/dt$ and λ as calculated above, Eq. **3** explains 83% of the variance in the 1981 to 2014 warming rate across all ensemble members of our CMIP5/6 model subset. Most of the explanatory power comes from variations in λ: Holding κ and $d(\mathrm{ERF})/dt$ fixed at ensemble-mean values, Eq. **3** still explains 58% of the variance across ensemble members. That is, variations in λ (and thus EffCS) largely govern the global warming rate, with variations in κ playing a secondary role. There is little correlation between λ and κ on the timescales considered here (*Materials and Methods*), so we treat them as independent for our purposes.

Using the regression between EffCS and the 1981 to 2014 warming rate derived from the eight-model subset (Fig. 1*D*), the observed warming rate of 0.18 (0.15 to 0.21) °C dec^{-1} implies EffCS = 2.3 (1.9 to 2.7) °C. While on the low end of the CMIP5/6 models (Fig. 1*D*), this implied value of EffCS is in good agreement with a recent observational estimate (19) of EffCS = 2.0 (1.5 to 3.1) °C based on global energy imbalance calculated from a merged satellite dataset (53) in combination with ERF estimates from IPCC AR6 (2) and HadCRUT5 temperature observations over 1985 to 2014. The CMIP5/6-based relationship between EffCS and warming rate thus compares well with observations.

Importantly, EffCS may be different from ECS, which is given by

$$\mathrm{ECS} = -\frac{\mathrm{ERF}_{2\times}}{\lambda_{2\times}}, \quad [4]$$

owing to the fact that the radiative feedback λ governing recent warming may be different from the radiative feedback $\lambda_{2\times}$ governing the equilibrium response to CO_2 doubling if warming patterns differ between the two timescales. Given that ECS is a measure of the equilibrium climate response to CO_2 forcing, it is worth considering why it is highly correlated with the rate of transient warming over 1981 to 2014 in CMIP5/6 models (Fig. 1 *A* and *B*). The reason appears to be that values of ECS and ensemble-mean EffCS are nearly identical for each of the CMIP5/6 models (Fig. 1*C*); EffCS is similar to but slightly smaller than ECS for most of the GCMs, with a high correlation between them ($r^2 = 0.70$).

These findings are consistent with the fact that the spatial patterns of historical warming (setting EffCS over 1981 to 2014) and equilibrium warming under abrupt CO_2 forcing (setting ECS) are similar in CMIP5/6 models (Fig. 2 *A* and *B*) (17); both are characterized by relatively weak spatial gradients in SST trends. That is, the relationship between ECS and the 1981 to 2014 warming rate, which forms the basis for the observational constraint, reflects similar patterns of transient and equilibrium warming within the coupled CMIP5/6 models, corresponding to a relatively small pattern effect (i.e., values of EffCS governing recent warming are comparable to values of ECS governing long-term warming).

As noted in the introduction, the observed SST trend pattern over 1981 to 2014 (Fig. 2*C*) is distinct from patterns simulated by the coupled CMIP5/6 models (17, 41, 42). With strong warming in the western tropical Pacific Ocean (a region of negative feedbacks) and cooling in the eastern Pacific and Southern Oceans (regions of positive feedbacks), the observed pattern should favor a low value of EffCS (8, 9, 14, 16, 17, 19–27) and thus a reduced global warming rate (Eq. **3**). This observed pattern of warming is also distinct from the long-term warming pattern we expect under CO_2 forcing (2), suggesting that the relationship between EffCS (governing recent warming) and ECS (governing long-term warming) in nature may be different from that simulated by CMIP5/6 models. In the next section, we consider how model SST trend biases may, in turn, bias the warming-sensitivity relationship which forms the basis for the observational constraint.

Impact of Model SST Trend Biases on the Warming-Sensitivity Relationship

To quantify the impact of the SST trend pattern on global warming rate, we make use of *amip* simulations wherein the same subset of eight AGCMs are run with prescribed time-evolving observed SSTs and SICs while all radiative forcing agents are varied as in the corresponding *historical* simulations. The *amip* simulations refer to the Atmospheric Model Intercomparison Project (AMIP II) DECK experiments performed as part of CMIP6 (36); we perform our own *amip*-style simulation for CESM1-CAM5. In combination with the RFMIP simulations, these simulations allow us to calculate λ and EffCS using regression over the period 1981 to 2014 as described above (see also refs. 14, 17, and 19).

Across the eight AGCMs, the observed 1981 to 2014 SST trend pattern produces an average value of EffCS = 2.1 °C (range 1.3 to 3.2 °C)—in good agreement with EffCS derived from global energy budget observations (19) and implied by the observed global warming rate (Figs. 1 *C* and *D*). This EffCS value is lower than the average EffCS simulated by the same coupled GCMs over 1981 to 2014. With identical atmospheric physics

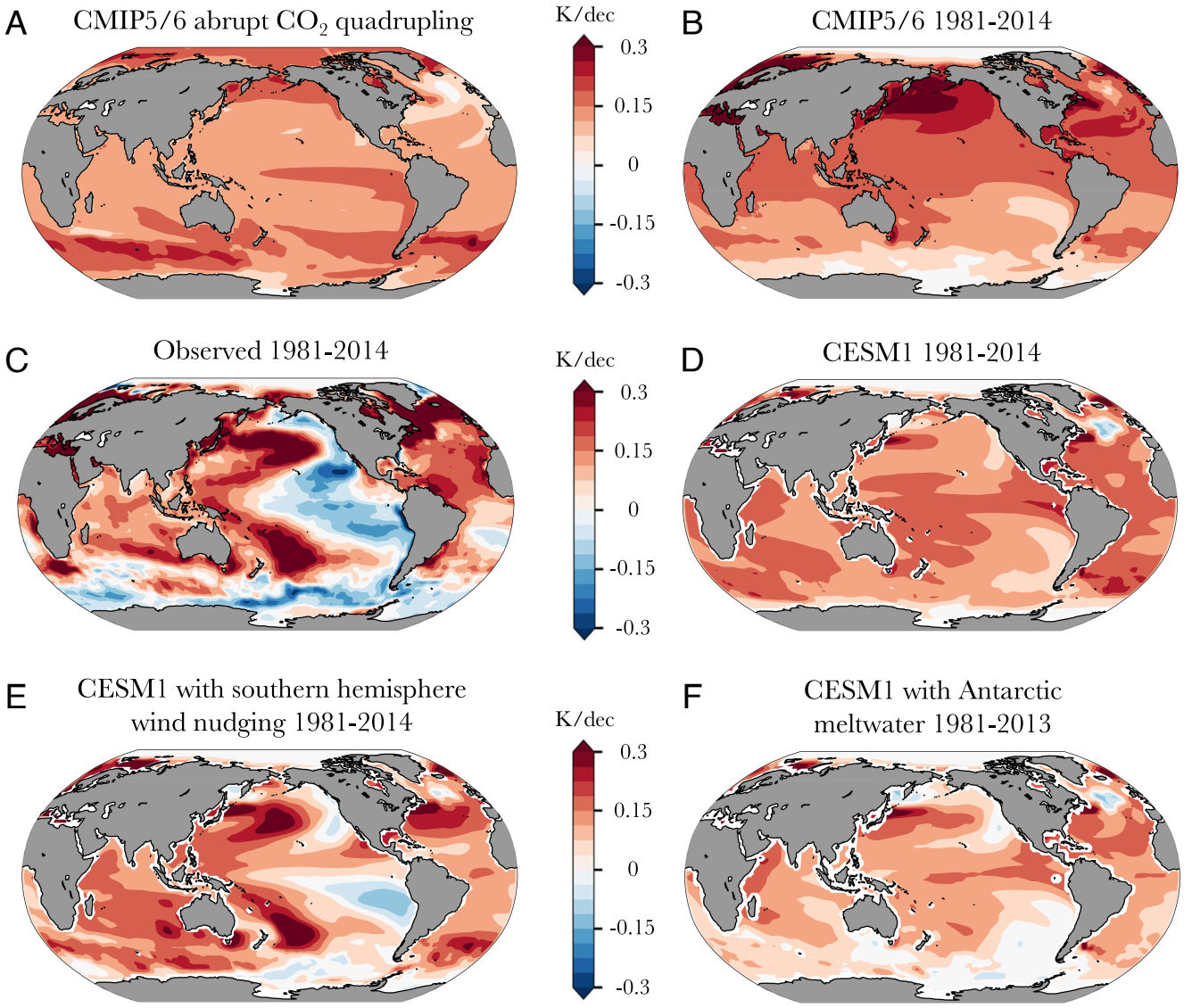

Fig. 2. SST trends in CMIP5/6 models and observations. SST trend patterns for (*A*) CMIP5/6 models over years 1 to 150 following abrupt CO_2 quadrupling (CMIP5/6 *abrupt4xCO2* simulations from which ECS is calculated). (*B*) CMIP5/6 models over 1981 to 2014 (CMIP5/6 *historical* simulations from which EffCS is calculated). (*C*) Observations over 1981 to 2014 (from *amip*). (*D*) CESM1-CAM5 over 1981 to 2014. (*E*) CESM1-CAM5 over 1981 to 2014 with Southern Hemisphere high latitude wind nudging. (*F*) CESM1-CAM5 over 1981 to 2013 with Antarctic meltwater fluxes.

in AGCM and coupled GCM versions of each model, EffCS differences are due only to differences in observed and simulated SST and SIC trend patterns (14, 17, 19).

For the coupled GCMs with low values of ECS (GISS-E2-1-G, MIROC6, NorESM2-LM), 1981 to 2014 EffCS values are similar for AGCM and coupled GCM simulations (Fig. 1*C*). However, for all other GCMs in our subset (CanESM5, CNRM-CM6-1, HadGEM3-GC31-LL, IPSL-CM6A-LR, CESM1-CAM5), 1981 to 2014 EffCS values in AGCMs are substantially lower than they are in the same coupled GCMs, with AGCM values being at the edge of or even below the range of EffCS values generated by internal variability in the coupled model historical simulations. This suggests that the observed SST trend pattern (Fig. 2*C*) reflects an extreme phase of internal variability, a forced response not captured by the coupled GCMs, or a combination of both (17, 42). A possible reason for the larger differences between AGCM and coupled GCM values of EffCS in high-ECS models is that ECS differences across models stem largely from model differences in cloud feedbacks in the eastern tropical Pacific and Southern Oceans (35). Thus, observed cooling in these regions over 1981 to 2014 reduces the value of EffCS more for models with higher ECS, while leaving the value of EffCS relatively unchanged for models with lower ECS. Further examination of CESM1-CAM5 shows that the regression of local SST trends onto either the global warming trend or EffCS over 1981 to 2014 across ensemble members highlights the eastern tropical Pacific and Southern Oceans as key regions governing the warming rate and EffCS (*SI Appendix*, Fig. S2).

The larger values of EffCS in the coupled GCMs relative to AGCMs suggests that at least a portion of the reason the coupled GCMs overestimate warming over 1981 to 2014 is that they fail to simulate the observed SST trend patterns—rather than simply having too-high values of ECS (or TCR). Moreover, it suggests that if the coupled GCMs were able to correctly simulate the observed warming patterns, they would produce lower values of EffCS (as shown by their AGCM simulations) and thus reduced

1981 to 2014 warming rates. In other words, CMIP5/6 models share a common bias in their ability to simulate the observed SST trend pattern which increases their values of EffCS and thus their rate of warming over recent decades—directly biasing their simulated relationship between warming rate and ECS on which observational constraints are based.

Correcting for SST Trend Pattern Biases in Observational Constraints

We next estimate the global-mean warming each GCM would produce if it correctly simulated the observed 1981 to 2014 SST trend pattern. To do so, we multiply the value of EffCS derived from the AGCM simulations by the regression coefficient between the EffCS and the 1981 to 2014 warming rate derived from all ensemble members in the eight-GCM subset (diamonds in Fig. 1*D* and *Materials and Methods*). The results suggest that each of the eight CMIP5/6 models would have produced warming near the observed warming rate had it simulated the observed SST trend pattern. Thus, once biases in SST trend patterns are accounted for, there is little correlation between the 1981 and 2014 warming rate and ECS (Fig. 3*A*). The average warming rate correction across the eight GCMs is −0.09 °C dec^{-1}, with larger reductions in warming rates (and EffCS) for models with higher ECS (Figs. 1*C* and 3*A*).

We conclude that observed warming is consistent with a wide range of ECS values, and that by failing to account for biases in coupled GCM SST trend patterns, the proposed observational constraint biases estimates of ECS toward low values. Similar results hold if we instead use the regression between 1981 and 2014 EffCS and warming rate derived from each GCM separately to estimate the warming rate consistent with AGCM EffCS values, but uncertainties are larger owing to larger uncertainty in the regression, particularly for models with few ensemble members (*SI Appendix*, Figs. S3 and S4).

As another method to estimate warming rates in the eight GCMs when correcting for biases in SST trend patterns, we use Eq. **3** with values of λ derived from each model's AGCM simulation (*Materials and Methods*). Once again, the results suggest that each of the eight CMIP5/6 models would have produced warming near the observed warming rate had they simulated the observed SST trend pattern, leaving little correlation between the 1981 and 2014 warming rate and ECS (Fig. 3*B*). The average warming rate correction across the eight GCMs is −0.05 °C dec^{-1} with a larger impact for models with higher ECS, once again. This supports our conclusion that observed warming is consistent with a wide range of ECS values, and that the proposed observational constraint biases estimates of ECS toward low values; similar results hold for constraints on TCR (*SI Appendix*, Figs. S1 and S4). It also suggests that observed global warming has been slowed by the unique SST trend pattern over recent decades (Fig. 2*C*) and that warming would have been more rapid had the pattern been more similar to that simulated by CMIP5/6 models (Fig. 2*B*).

Simulations with a Two-Layer Energy Balance Model (EBM). The results presented so far rely on diagnostic interpretation of CMIP5/6 output and on inferences of GCM warming rates had they correctly simulated the observed 1981 to 2014 SST trend pattern and associated EffCS. Here we evaluate the robustness of this interpretation within the context of a widely used EBM (refs. 54–56) which represents the Earth as two interacting layers—one representing all surface components of the climate

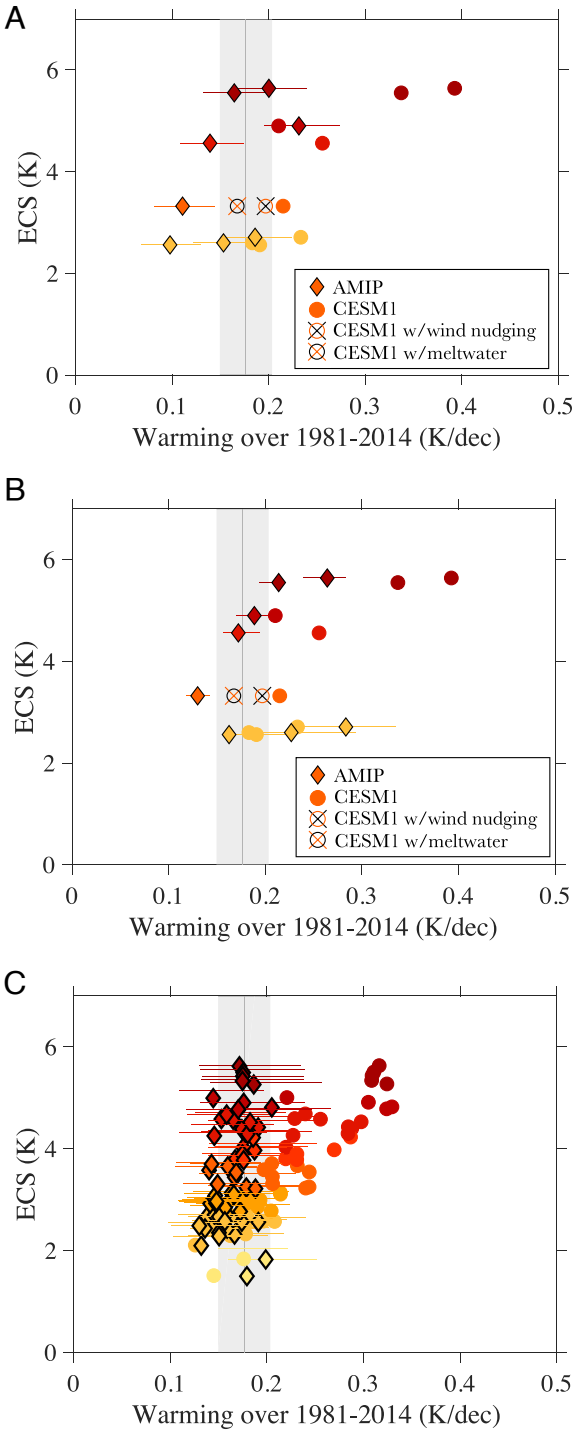

Fig. 3. Relationships between ECS and the 1981 to 2014 warming rate with (diamonds) and without (circles) accounting for observed warming patterns. ECS vs warming rate for (*A*) CMIP5/6 eight-model subset, with circles showing uncorrected warming rates (from Fig. 1*B*) and diamonds showing corrected warming rates estimated using AGCM values of EffCS and the relationship between EffCS and warming (Fig. 1*D*); horizontal lines show 5 to 95% confidence ranges from uncertainty in the fit. (*B*) CMIP5/6 eight-model subset, with circles showing uncorrected warming rates (from Fig. 1*B*) and diamonds showing corrected warming rates estimated using AGCM values of λ and Eq. **3**, with horizontal lines showing uncertainty ranges reflecting the spread in κ across ensemble members. (*C*) Relationship between ECS and warming rate in two-layer EBM simulations with circles showing uncorrected warming rates and diamonds showing corrected warming rates using observed values of EffCS (19) (*SI Appendix*, Fig. S6), with a median of 2 °C and horizontal lines showing 5 to 95% confidence ranges illustrating 1.5 to 3.1 °C. Gray shading shows observational estimates (5 to 95% range) of observed warming rate (HadCRUT5, ref. 45).

system, including the near-surface atmosphere, ocean mixed layer, cryosphere, and land; and one representing the ocean below the mixed layer. The EBM predicts the surface temperature response to ERF through a representation of the efficiency of radiative response (governed by λ), the efficiency of ocean heat uptake, and the efficacy of ocean heat uptake which allows feedbacks to change over time as in coupled GCMs (*Materials and Methods*). This EBM was used extensively in IPCC AR6, including for constraining global temperature projections (see climate model "emulators" in refs. 2 and 4). Here it provides a predictive physical model with all of the necessary ingredients to test the robustness of the above results derived from diagnostic analyses of CMIP5/6 models.

We fit the EBM parameters to the CMIP5/6 *abrupt4xCO2* simulations of all models used in the analysis above (*Materials and Methods*; *SI Appendix*). For each CMIP5/6 model parameter set, we run the EBM over the period 1850 to 2014 using the timeseries of historical ERF calculated as an average over the eight-model subset as described above, and we calculate EffCS over 1981 to 2014 using Eqs. **1** and **2**. We also run the EBM under an abrupt increase in ERF representing CO_2 quadrupling (to calculate EBM values of ECS using regression over 150 y, as in the CMIP5/6 models).

The EBM produces features similar to the CMIP5/6 analysis seen in Fig. 1. There is a strong correlation between the 1981 to 2014 warming rate and ECS, with lower ECS values being more consistent with observations (Fig. 3*C* and *SI Appendix*, Fig. S5). This correlation is explained by the fact that 1981 to 2014 EffCS values, governing warming over that period, are similar to ECS values (*SI Appendix*, Fig. S5); EffCS tends to be slightly smaller than ECS owing to the ocean heat uptake efficacy parameter being larger than one for most CMIP5/6 models (*SI Appendix*), allowing feedbacks under transient warming to be slightly more negative than at equilibrium. Differences in EffCS explain a large fraction of the variance in the 1981 to 2014 warming rate ($r^2 = 0.88$); values of EffCS near 2 °C tend to produce warming rates in line with observations, while higher values of EffCS produce too much warming (*SI Appendix*, Fig. S5). The remaining variations in EBM warming rates come from differences in ocean model parameters (*Materials and Methods*), but differences in forcing do not contribute here because we have used the same historical ERF for all parameter sets. The regression between EffCS and the 1981 to 2014 warming rate also nearly matches that found from the eight-model subset and agrees well with the relationship between EffCS and the 1981 to 2014 warming rate derived from observational constraints (*SI Appendix*, Fig. S5).

We next consider how EBM simulations of the 1981 to 2014 warming rate change when we introduce a linear trend in λ (*Materials and Methods*), representing an idealization of trends in λ over recent decades as simulated by AGCMs forced by observed warming patterns (8, 14, 17, 19, 25), such that EffCS over 1981 to 2014 becomes equal to the value EffCS = 2.0 °C (with bounds of 1.5 to 3.1 °C also tested) estimated from global energy budget observations (19). This produces a substantial decrease in EffCS for high ECS models, but little change in EffCS for low ECS models (diamonds in *SI Appendix*, Fig. S5), similar to differences seen in coupled GCM and AGCM versions of CMIP5/6 models (Fig. 1*C*). The result is that the EBM produces warming near the observed rate for all CMIP5/6 model parameter sets, in line with expectations based on the regression between EffCS and warming rate (Fig. 3*C* and *SI Appendix*, Fig. S5). The average warming rate correction across the subset of eight models is −0.06 °C dec^{-1}, with larger reductions in warming rates (and EffCS) for models with higher ECS, similar to our analysis using CMIP5/6 models above.

The relationship between ECS and the warming rate when imposing observed EffCS within the EBM is shown in Fig. 3*C*. Each CMIP5/6 model parameter set produces warming near the observed 1981 to 2014 warming rate, with little correlation between warming rate and ECS. These results show that the low value of EffCS produced by the observed 1981 to 2014 SST trend pattern implies warming in line with the observed global warming rate, regardless of the value of ECS. This supports our interpretation that observed warming is consistent with a wide range of ECS values once accounting for the observed SST trend pattern and its associated low EffCS. Similar results hold for comparisons of warming rates and TCR (*SI Appendix*, Fig. S5).

Simulations with a Coupled GCM Nudged toward Observed Warming Patterns. Finally, we evaluate the robustness of our results using two sets of CESM1-CAM5 simulations wherein the coupled model is nudged toward the observed 1981 to 2014 SST trend pattern in physically plausible ways. The first set of simulations, performed by Dong et al. (57) based on methods developed in Blanchard-Wrigglesworth et al. (58), involves nudging Southern Hemisphere tropospheric winds (above the boundary layer) poleward of 40°S to match the ERA-Interim Reanalysis over the period 1981 to 2014; five ensemble members were run, which we average together for comparison to the CESM1-CAM5 ensemble mean response. The second set of simulations, performed by Dong et al. (52) and Pauling et al. (59), involves adding meltwater to the Southern Ocean subsurface to represent discharge due to mass imbalance of the Antarctic ice sheet over 1981 to 2013 (an effect not represented in CMIP5/6 *historical* simulations); nine ensemble members were run, which we average together for comparison to the CESM1-CAM5 ensemble mean response. In both sets of simulations, the SST trend pattern more closely matches observations, with some cooling in the Southern Ocean and eastern tropical Pacific Ocean and with warming in the western Pacific Ocean becoming relatively larger (Fig. 2 *E* and *F*); see ref. 57 for a discussion of the atmospheric teleconnection pathways by which these southern high latitude forcings influence tropical SST patterns.

Using Eqs. **1** and **2** as before, we find that both sets of simulations produce smaller values of EffCS than the ensemble mean of CESM1-CAM5 *historical* simulations (Fig. 1*C*), bringing EffCS nearer to that estimated from global energy budget observations (19). In turn, both sets of simulations show reduced global warming rates (Fig. 1*D*) that are more in line with observations. The relationship between EffCS and warming rate in these simulations also approximately follows expectations based on the regression between EffCS and warming rate derived from either the eight-model subset (Fig. 1*D*) or CESM1-CAM5 (*SI Appendix*, Fig. S3). However, despite similar changes to EffCS, Antarctic meltwater forcing produces a larger reduction in global warming rate than Southern Hemisphere wind forcing in this model owing to an increase in ocean heat uptake efficiency (κ) that works together with feedback (λ) changes to slow the warming (52). Similar results hold for comparisons of warming rates and TCR (*SI Appendix*, Figs. S1 and S4). These findings support the interpretation above that EffCS (rather than ECS or TCR) governs the global warming rate over 1981 to 2014, and that when coupled GCMs more accurately replicate observed SST trend patterns, they produce lower EffCS and thus slower global warming, in line with observations.

Discussion and Conclusions

The results presented here suggest that high-sensitivity CMIP5/6 models produce too much post-1970s warming in part due to their failure to simulate observed SST trend patterns, which in turn leads to model values of EffCS that are too high compared to the observed EffCS of around 2 °C over this period. Because GCMs with high values of ECS and TCR are able to produce values of EffCS near 2 °C when forced by observed SSTs over 1981 to 2014 (Fig. 1*C* and *SI Appendix*, Fig. S1*C*), we estimate that even those high-sensitivity GCMs could produce global warming rates in line with observations if they were able to better simulate observed SST trend patterns (Figs. 1*D* and 3 *A* and *B*). This is a bias in the GCM-based relationship between post-1970s warming and climate sensitivity metrics which causes the proposed observational (or "emergent") constraint to be biased toward low values of climate sensitivity. While published constraints (18, 32–34) may still reflect useful lower bounds on ECS and TCR, we find that they are consistent with wide ranges of ECS and TCR extending to higher values than previously recognized. While not a focus here, model biases in historical radiative forcing (e.g., refs. 60 and 61) could also impart biases in the modeled warming-sensitivity relationship on which the observational constraint is based.

It is worth considering the implications of these results for the recent climate sensitivity assessments that substantial narrowed climate sensitivity uncertainty by estimating *very likely* ranges of around 2 to 5 °C for ECS (2, 3) and 1.2 to 2.4 °C for TCR (2). That the observed rate of recent warming cannot be used to constrain climate sensitivity means we must rely on other lines of evidence. Sherwood et al. (3) employed a Bayesian framework to combine several independent lines of evidence for ECS, with paleoclimate observations and process understanding of climate feedbacks providing strong constraints on the high end. Importantly, that assessment did not use observational (or emergent) constraints based on recent warming, so our findings do not affect that assessed ECS range.

However, without employing a formal Bayesian framework, AR6 relied on observational constraints based on global temperature changes as the strongest constraint on the upper ends of the ECS and TCR ranges (while many different lines of evidence support the lower ends of the ranges). Together with the recent result that the climate response to the Mt. Pinatubo eruption also does not provide a reliable observational constraint on ECS (62), our findings suggest that the upper end of the climate sensitivity range is less well supported than it was within AR6, particularly for TCR which relied more heavily on this type of observational constraint. There still remain other observational constraints providing evidence against high ECS values, most notably those based on proxy-estimated cooling at the Last Glacial Maximum (2), but for now, the Bayesian framework of Sherwood et al. (3) may provide the most robust support for a 2 to 5 °C *very likely* range of ECS. A final implication is that the evaluation of model ECS, TCR, and future warming based on their performance in historical simulations (e.g., refs. 34, 63, and 64) must also account for different SST trend patterns between observations and models, with our results suggesting that even high sensitivity models are compatible with observed warming. This too suggests that testing in paleoclimate settings (e.g., ref. 65) may provide a more useful evaluation of model climate sensitivity and long-term warming.

Important questions remain, including: i) why do CMIP5/6 models fail to replicate observed warming patterns over recent decades, and how can this model bias be corrected? And, ii) for how long will the observed pattern of warming over recent decades continue into the 21st century? Model-observation discrepancies may be due to model deficiencies in simulating internal variability and/or historical forced responses. Paleoclimate proxy and instrumental data suggest that tropical Pacific multidecadal variability may be substantially larger than that produced by coupled GCMs (e.g., refs. 66–68), which seems consistent with the observed 1981 to 2014 SST trend pattern resembling an extreme phase of the Interdecadal Pacific Oscillation mode of variability (e.g., refs. 41, 42, 68, and 69). Alternatively, several other model deficiencies have been proposed to contribute to the SST trend pattern over recent decades including model biases in trends in the Southern Annular Mode, potentially due to a misrepresentation of ozone depletion (e.g., refs. 57, 70, and 71); missing Antarctic meltwater fluxes (e.g., refs. 52, 57, 59, and 72); a misrepresentation of tropospheric aerosol forcing, which can affect Pacific trade winds (e.g., ref. 73); model biases in Atlantic Ocean SSTs that limit the ability of the Atlantic basin to affect Pacific trade winds (74); model biases in the transient response of the tropical Pacific to CO_2 forcing (e.g., refs. 75 and 76) or volcanic forcing (16); and limitations associated with model resolution (e.g., ref. 77).

Our findings do not depend on the source of the discrepancy between CMIP5/6-simulated and observed warming patterns because radiative feedbacks and EffCS depend only on SST and SIC patterns, regardless of how those patterns arise (e.g., refs. 78 and 79). But implicit in our use of AMIP simulations to estimate how the SST trend pattern has influenced global warming rates is that the pattern itself is largely independent of ECS. Recent studies argue that models with more-positive subtropical low-cloud feedbacks (and thus higher ECS) may better replicate the observed cooling of the eastern tropical Pacific (e.g., ref. 80), at least when resulting from Southern Ocean cooling (52, 57). This potential link between ECS and the SST trend pattern would further support our finding that high ECS models can produce low values of EffCS, and thus slow global warming rates.

The results presented here suggest that changes in EffCS have the capacity to substantially affect the global warming rate and that a low value of EffCS driven by a unique SST trend pattern has slowed global-mean warming over recent decades, relative to what it would have been had the pattern been more spatially uniform. However, more work is needed to determine whether CMIP5/6 models with high ECS (above ∼4 °C) are capable of producing the observed SST trend pattern and associated low EffCS needed to bring their simulated global warming rates in line with observations over recent decades. It would be valuable to perform similar wind nudging and/or Antarctic meltwater flux simulations, shown here for CESM1-CAM5, using high ECS models.

These results reinforce previous findings that global warming will depend on how the SST trend pattern evolves in the future (e.g., refs. 52 and 81–83). Our findings suggest that if the observed 1981 to 2014 pattern continues over the 21st century, then the value of EffCS governing future warming will remain near 2 °C. This would produce 21st century global warming near the lower end of IPCC AR6 projections (*SI Appendix*, Fig. S7), which assume a *very likely* range of ECS of 2 to 5 °C (2). However, if enhanced warming of the eastern tropical Pacific and Southern Oceans were to emerge in the future—a pattern projected by GCM simulations of the 21st century and supported by paleoclimate proxy evidence (e.g., refs. 2 and 84)—then EffCS would increase, resulting in an increase in the rate of global warming (*SI Appendix*, Fig. S7). The degree to

which EffCS could increase depends on the magnitude of the warming in the eastern tropical Pacific and Southern Oceans, and on the magnitude of the radiative feedbacks in those regions. Because observed post-1970s warming has a unique spatial pattern that does not appear to be representative of the long-term response to greenhouse-gas forcing, it does not preclude the possibility that high values of EffCS are possible for the future, potentially leading to future warming near or even above the upper end of IPCC AR6 projections if ECS turns out to be on the high end. How the pattern of warming will evolve in the future thus represents a major source of uncertainty in climate projections.

Developing improved understanding of the causes of the observed SST trend pattern over recent decades and better constraints on how those patterns will evolve in the future is a major challenge for climate science with direct implications for how we interpret the historical warming record and project 21st century warming. We could, for instance, see an increase in the climate's sensitivity to greenhouse-gas forcing if SST trend patterns evolve to become more similar to those projected by models. For now, climate model biases in historical SST trend patterns suggest that caution is needed in the use of models to derive observational (or emergent) constraints on climate sensitivity or future warming based on the rate of global warming over recent decades.

Materials and Methods

Linear Regression Methods. We use OLS regression to calculate 1981 to 2014 warming rates and the regression of climate sensitivity metrics (ECS, TCR) against 1981 to 2014 warming rates using ensemble-mean values (Fig. 1 *A* and *B* and *SI Appendix*, Fig. S1 *A* and *B*). To estimate ECS and TCR from the warming-sensitivity relationships (Fig. 1*A* and *SI Appendix*, Fig. S1*A*), we calculate a linear fit of ECS (or TCR) versus 1981 to 2014 warming rate and use the parameters of that fit to estimate ECS (or TCR) given the observed warming rate (HadCRUT5, ref. 45) over 1981 to 2014. Uncertainties in ECS and TCR reflect 5 to 95% confidence ranges of fit parameter values.

For the calculation of the effective feedback λ from the regression of $N-$ ERF against T (Eq. **1**), the presence of error in the predictor variable biases OLS regression toward zero (regression dilution). To correct for this, we use Deming regression, a total least squares regression method, to calculate λ. We estimate the ratio of error variances (variance of global average top-of-atmosphere radiation and variance in global average surface temperature) to be approximately 10 $W^2m^{-4}K^{-2}$ based on AGCM simulations using SSTs fixed at pre-industrial conditions. We use OLS regression for all regressions based on the two-layer EBM, which does not represent internal variability. Within CESM1-CAM5, moderate correlations between EffCS and warming rate over 1981 to 2014 are found when using the CAM5 Green's function (22) combined with SST trend patterns to estimate radiative feedback and EffCS (*SI Appendix*, Fig. S2).

ERF. Historical ERF is calculated for each of the eight models in our subset using RFMIP (46) simulations. The historical ERF is diagnosed as the global top-of-atmosphere radiation anomaly in *piClim-histall* simulations (wherein SSTs and SICs are fixed to pre-industrial values while all radiative forcing agents are varied as in the corresponding CMIP6 *historical* simulations) relative to *piClim-control* simulations (wherein SSTs, SICs, and all radiative forcing agents are fixed to pre-industrial values). A small correction (2, 48) is made to remove the radiative response to global near-surface air temperature change T (mostly land warming) by subtracting $\lambda_{2\times}T$, where $\lambda_{2\times}$ is estimated from *abrupt4xCO2* simulations (35). For all RFMIP simulations, the ensemble mean is used when more than one member of the simulation exists. CMIP5/6 model values of ERF for CO_2 doubling ($ERF_{2\times}$) have been estimated using the standard approach of extrapolating to zero global temperature change the regression between global top-of-atmosphere energy imbalance and global temperature change over 150 y of abrupt CO_2 quadrupling simulations, scaled by a factor of a half to account for CO_2 doubling (35, 44).

Correcting for SST Trend Pattern Biases. For the first method of estimating the warming each GCM would produce if it correctly simulated the observed 1981 to 2014 SST trend pattern (Fig. 3*A*), we first calculate a linear fit (OLS regression) of EffCS versus 1981 to 2014 warming rate from all ensemble members of the eight-GCM subset (Fig. 1*D*). We then use that fit to estimate the warming rate given EffCS derived from each AGCM simulation (diamonds in Figs. 1*D* and 3*A*). Uncertainties (horizontal lines in Fig. 3*A*) reflect 5 to 95% confidence ranges of fit parameter values.

For the second method of estimating the warming each GCM would produce if it correctly simulated the observed 1981 to 2014 SST trend pattern (Fig. 3*B*), we use Eq. **3** with values of λ derived from each model's AGCM simulation. In the eight-model ensemble considered here, the average correlation between λ and κ across historical ensemble members is small (average $r^2 = 0.25$), and models disagree on the sign of the correlation. Without a deeper understanding of how variations in λ and κ are related, we assume they can be varied independently and use ensemble-mean values of κ for each model in this estimate. To evaluate the degree to which variations in κ could affect the results, uncertainties (horizontal lines in Fig. 3*B*) are generated by using the highest and lowest values of κ from the ensemble members of each model in this calculation.

Two-Layer EBM. The two-layer EBM (refs. 54–56) evolves surface temperature according to the following equations:

$$C\frac{dT}{dt} = \lambda T + \mathrm{ERF} - \varepsilon\gamma(T - T_0),$$
$$C_0\frac{dT_0}{dt} = \gamma(T - T_0), \qquad [5]$$

where T is the temperature anomaly of the upper layer, representing the global surface temperature anomaly; T_0 is the temperature anomaly of the lower layer; ERF is the effective radiative forcing, as above; C is the effective heat capacity of the upper layer (representing the ocean mixed layer, land, and atmosphere); C_0 is the effective heat capacity of the lower layer (representing the ocean below the mixed layer); γ represents the efficiency of vertical heat transport between upper and lower layers; and ε is the efficacy of ocean heat uptake, which allows effective radiative feedbacks to change over time as represented by coupled GCMs. Note that in the limit of $C_0 \gg C$, such that deep ocean temperature T_0 does not change much, these equations reduce to Eq. **3** with $\kappa = \varepsilon\gamma$.

We fit the two-layer EBM parameters to the *abrupt4xCO2* simulations of all CMIP5/6 models used in the analysis above using the fitting scheme developed by Lutsko and Popp (85), which was based on Geoffroy et al. (56) (see *SI Appendix* for parameter values). To simulate historical warming consistent with observational constraints on EffCS, we run the model using a wide range of linear trends in λ over the period 1981 to 2014 (starting from initial values of λ as fit to CMIP5/6 models and changing linearly with time) and calculate EffCS over this period (using Eq. **1**) for each. We then select the simulations that correspond to EffCS values of 2.0 °C, 1.5 °C, and 3.1 °C (50%, 5%, and 95% intervals of the observationally constrained EffCS from ref. 19). See *SI Appendix* for details regarding the 21st century EBM simulations under different assumptions about how EffCS will evolve in the future.

Data, Materials, and Software Availability. netcdf files and code data have been deposited in Dryad (https://doi.org/10.5061/dryad.zgmsbcckd) (86).

ACKNOWLEDGMENTS. K.C.A., C.P., and L.C.H. were supported by Department of Energy (DOE) Award DE-SC0022110, NSF Award AGS-1752796, and National Oceanic and Atmospheric Administration (NOAA) Modeling, Analysis, Predictions and Projections Program Award NA20OAR4310391. K.C.A. was supported by an Alfred P. Sloan Research Fellowship (Award FG-2020-13568) and a Calvin Professorship in Oceanography. L.C.H. was supported by the Tamaki Foundation.

T.A. was supported by the Met Office Hadley Centre Climate Programme funded by the UK Department of Business, Energy and Industrial Strategy and the European Union's Horizon 2020 research and innovation programme under grant agreement 820829. M.F.S. was supported by NSF Award AGS-2141728. E.B.-W. was supported by NSF Award OPP-2213988. R.C.J.W. was supported by the Swiss NSF Award PCEFP2_203376 and NSF Award AGS-2203543. I.M. was supported by Future Investigators in NASA Earth and Space Science and Technology grant 80NSSC20K1657. Y.D. was supported by the NOAA Climate and Global Change Postdoctoral Fellowship Program, administered by University Corporation for Atmospheric Research's Cooperative Programs for the Advancement of Earth System Science under award NA210AR4310383. Work by S.P.-C. was supported by the Regional and Global Model Analysis Program of the Office of Science and was performed under the auspices of the U.S. DOE by Lawrence Livermore National Laboratory under Contract DE-AC52-07NA27344. We also acknowledge high-performance computing support from Cheyenne (https://doi.org/10.5065/D6RX99HX) provided by the National Center for Atmospheric Research's Computational and Information Systems Laboratory, sponsored by the NSF. This is International Pacific Research Center (IPRC) publication 1614 and School of Ocean and Earth Science and Technology (SOEST) contribution 11755.

Author affiliations: [a]Department of Atmospheric Sciences, University of Washington, Seattle, WA 98195; [b]School of Oceanography, University of Washington, Seattle, WA 98195; [c]Department of Climate, Meteorology, and Atmospheric Sciences, University of Illinois, Urbana-Champaign, Champaign, IL 61801; [d]Department of Earth Sciences and Environmental Change, University of Illinois, Urbana-Champaign, Champaign, IL 61801; [e]Cooperative Institute for Research in Environmental Sciences, University of Colorado, Boulder, CO 80309; [f]Scripps Institution of Oceanography, La Jolla, CA 92093; [g]Department of Physics, University of Otago, Dunedin, NZ 9016; [h]Institute for Atmospheric and Climate Science, ETH Zurich, Zurich, CH 8092; [i]Met Office Hadley Centre, Exeter EX1 3PB, United Kingdom; [j]Department of Oceanography and International Pacific Research Center, School of Ocean and Earth Science and Technology, University of Hawai'i at Mānoa, Honolulu, HI 96822; [k]Program for Climate Model Diagnosis and Intercomparison, Lawrence Livermore National Laboratory, Livermore, CA 94550; [l]Department of Applied Physics and Applied Mathematics, Columbia University, New York, NY 10027; [m]Priestley International Centre for Climate, University of Leeds, Leeds LS2 9JT, United Kingdom; and [n]National Centre for Atmospheric Science, University of Reading, Reading RG6 6ET, United Kingdom

Author contributions: K.C.A. and C.P. designed research; K.C.A., C.P., Y.D., L.C.H., E.B.-W., A.G.P., R.C.J.W., T.A., M.F.S., S.P.-C., I.M., P.M.F., and J.M.G. performed research; K.C.A., C.P., Y.D., L.C.H., E.B.-W., A.G.P., R.C.J.W., T.A., M.F.S., S.P.-C., and I.M. analyzed data; and K..A. wrote the paper.

1. M. R. Grose, J. Gregory, R. Coleman, T. Andrews, What climate sensitivity index is most useful for projections? *Geophys. Res. Lett.* **45**, 1559–1566 (2018).
2. P. Forster *et al*., "The earth's energy budget, climate feedbacks, and climate sensitivity" in *Climate Change 2021: The Physical Science Basis. Contribution of Working Group I to the Sixth Assessment Report of the Intergovernmental Panel on Climate Change*, V. Masson-Delmotte *et al*., Eds. (Cambridge University Press, 2021).
3. S. C. Sherwood *et al*., An assessment of earth's climate sensitivity using multiple lines of evidence. *Rev. Geophys.* **58**, e2019RG000678 (2020).
4. J. Y. Lee *et al*., "Future global climate: Scenario-based projections and near-term information" in *Climate Change 2021: The Physical Science Basis. Contribution of Working Group I to the Sixth Assessment Report of the Intergovernmental Panel on Climate Change*, V. Masson-Delmotte *et al*., Eds. (Cambridge University Press, 2021).
5. M. Collins *et al*., "Long-term climate change: Projections, commitments and irreversibility" in *Climate Change 2013: The Physical Science Basis. Contribution of Working Group I to the Fifth Assessment Report of the Intergovernmental Panel on Climate Change* T. F. Stocker *et al*., Eds. (Cambridge University Press, Cambridge, United Kingdom/New York, NY, 2013).
6. A. Otto *et al*., Energy budget constraints on climate response. *Nat. Geosci.* **6**, 415–416 (2013).
7. N. Lewis, J. A. Curry, The implications for climate sensitivity of AR5 forcing and heat uptake estimates. *Clim. Dyn.* **45**, 1009–1023 (2015).
8. J. M. Gregory, T. Andrews, Variation in climate sensitivity and feedback parameters during the historical period. *Geophys. Res. Lett.* **43**, 3911–3920 (2016).
9. C. Zhou, M. D. Zelinka, S. A. Klein, Impact of decadal cloud variations on the Earth's energy budget. *Nat. Geosci.* **9**, 871–874 (2016).
10. K. Marvel, G. A. Schmidt, R. L. Miller, L. Nazarenko, Implications for climate sensitivity from the response to individual forcings. *Nat. Clim. Change* **6**, 386–389 (2016).
11. K. C. Armour, Energy budget constraints on climate sensitivity in light of inconstant climate feedbacks. *Nat. Clim. Change* **7**, 331–335 (2017).
12. C. Proistosescu, P. Huybers, Slow climate mode reconciles historical and model-based estimates of climate sensitivity. *Sci. Adv.* **3**, e1602821 (2017).
13. N. Lewis, J. Curry, The impact of recent forcing and ocean heat uptake data on estimates of climate sensitivity. *J. Clim.* **3**, 6051–6071 (2018).
14. T. Andrews *et al*., Accounting for changing temperature patterns increases historical estimates of climate sensitivity. *Geophys. Res. Lett.* **45**, 8490–8499 (2018).
15. K. Marvel, R. Pincus, G. A. Schmidt, R. L. Miller, Implications for climate sensitivity from the response to individual forcings. *Geophys. Res. Lett.* **45**, 1595–1601 (2018).
16. J. M. Gregory, T. Andrews, P. Ceppi, T. Mauritsen, M. J. Webb, How accurately can the climate sensitivity to CO_2 be estimated from historical climate change? *Clim. Dyn.* **54**, 129–157 (2020).
17. Y. Dong *et al*., Biased estimates of equilibrium climate sensitivity and transient climate response derived from historical cmip6 simulations. *Geophys. Res. Lett.* **48**, e2021GL095778 (2021).
18. M. Winton *et al*., Climate sensitivity of GFDL's CM4.0. *J. Adv. Model. Earth Syst.* **12**, e2019MS001838 (2020).
19. T. Andrews *et al*., On the effect of changing SST patterns on historical radiative feedbacks. *J. Geophys. Res.: Atmos.* **127**, e2022JD036675 (2022).
20. K. C. Armour, C. M. Bitz, G. H. Roe, Time-varying climate sensitivity from regional feedbacks. *J. Clim.* **26**, 4518–4534 (2013).
21. T. Andrews, J. M. Gregory, M. J. Webb, The dependence of radiative forcing and feedback on evolving patterns of surface temperature change in climate models. *J. Clim.* **28**, 1630–1648 (2015).
22. C. Zhou, M. D. Zelinka, S. A. Klein, Analyzing the dependence of global cloud feedback on the spatial pattern of sea surface temperature change with a Green's function approach. *J. Adv. Model. Earth Syst.* **9**, 2174–2189 (2017).
23. P. Ceppi, J. M. Gregory, Relationship of tropospheric stability to climate sensitivity and earth's observed radiation budget. *Proc. Natl. Acad. Sci. U.S.A.* **114**, 13126–13131 (2017).
24. T. Andrews, M. J. Webb, The dependence of global cloud and lapse rate feedbacks on the spatial structure of Tropical Pacific warming. *J. Clim.* **31**, 641–654 (2018).
25. Y. Dong, C. Proistosescu, K. C. Armour, D. S. Battisti, Attributing historical and future evolution of radiative feedbacks to regional warming patterns using a Green's function approach: The preeminence of the Western Pacific. *J. Clim.* **32**, 5471–5491 (2019).
26. Y. Dong *et al*., Intermodel spread in the pattern effect and its contribution to climate sensitivity in CMIP5 and CMIP6 models. *J. Clim.* **33**, 7755–7775 (2020).
27. S. Fueglistaler, L. G. Silvers, The peculiar trajectory of global warming. *J. Geophys. Res.: Atmos.* **126**, e2020JD033629 (2021).
28. S. A. Klein, A. Hall, Emergent constraints for cloud feedbacks. *Curr. Clim. Change Rep.* **1**, 276–287 (2015).
29. A. Hall, P. Cox, C. Huntington, S. Klein, Progressing emergent constraints on future climate change. *Nat. Clim. Change* **9**, 269–278 (2019).
30. V. Eyring *et al*., Taking climate model evaluation to the next level. *Nat. Clim. Change* **9**, 102–110 (2019).
31. F. Brient, The potential for structural errors in emergent constraints. *Adv. Atmos. Sci.* **37**, 1–15 (2020).
32. D. Jiménez-de-la Cuesta, T. Mauritsen, Emergent constraints on earth's transient and equilibrium response to doubled CO_2 from post-1970s global warming. *Nat. Geosci.* **12**, 902–905 (2019).
33. F. J. M. M. Nijsse, P. M. Cox, M. S. Williamson, An emergent constraint on transient climate response from simulated historical warming in cmip6 models. *Earth Syst. Dyn.* **11**, 737–750 (2020).
34. K. B. Tokarska *et al*., Past warming trend constrains future warming in CMIP6 models. *Sci. Adv.* **12**, eaaz9549 (2020).
35. M. D. Zelinka *et al*., Causes of higher climate sensitivity in CMIP6 models. *Geophys. Res. Lett.* **47**, e2019GL085782 (2020).
36. V. Eyring *et al*., Overview of the coupled model intercomparison project phase 6 (CMIP6) experimental design and organization. *Geosci. Mod. Dev.* **9**, 1937–1958 (2016).
37. Z. Hausfather, K. Marvel, G. A. Schmidt, J. W. Nielsen-Gammon, M. Zelinka, Climate simulations: Recognize the 'hot model' problem. *Nature* **605**, 26–29 (2022).
38. P. M. Caldwell *et al*., Statistical significance of climate sensitivity predictors obtained by data mining. *Geophys. Res. Lett.* **41**, 1803–1808 (2014).
39. P. M. Caldwell, M. D. Zelinka, S. A. Klein, Evaluating emergent constraints on equilibrium climate sensitivity. *J. Clim.* **31**, 3921–3942 (2018).
40. B. M. Sanderson *et al*., The potential for structural errors in emergent constraints. *Earth Syst. Dyn.* **12**, 899–918 (2021).
41. S. McGregor *et al*., Recent walker circulation strengthening and pacific cooling amplified by Atlantic warming. *Nat. Clim. Change* **4**, 888–892 (2014).
42. R. C. J. Wills, Y. Dong, C. Proistosescu, K. C. Armour, D. S. Battisti, Systematic climate model biases in the large-scale patterns of recent sea-surface temperature and sea-level pressure change. *Geophys. Res. Lett.* **49**, e2022GL100011 (2022).
43. C. Smith *et al*., "The Earth's energy budget, climate feedbacks, and climate sensitivity supplementary material" in *Climate Change 2021: The Physical Science Basis. Contribution of Working Group I to the Sixth Assessment Report of the Intergovernmental Panel on Climate Change*, V. Masson-Delmotte *et al*., Eds. (Cambridge University Press, 2021).
44. I. Mitevski, L. M. Polvani, C. Orbe, Asymmetric warming/cooling response to CO_2 increase/decrease mainly due to non-logarithmic forcing, not feedbacks. *Geophys. Res. Lett.* **49**, e2021GL097133 (2022).
45. C. P. Morice *et al*., An updated assessment of near-surface temperature change from 1850: The HADCRUT5 data set. *J. Geophys. Res.: Atmos.* **126**, e2019JD032361 (2021).
46. R. Pincus, P. M. Forster, B. Stevens, The radiative forcing model intercomparison project (RFMIP): Experimental protocol for CMIP6. *Geosci. Mod. Dev.* **9**, 3447–3460 (2016).
47. T. Andrews *et al*., Effective radiative forcing in a GCM with fixed surface temperatures. *J. Geophys. Res.: Atmos.* **126**, e2020JD033880 (2021).
48. J. Hansen *et al*., Efficacy of climate forcings. *J. Geophys. Res.: Atmos.* **110**, D18104 (2005).
49. J. M. Gregory, M. J. F. B, The climate response to CO_2 of the Hadley Centre coupled AOGCM with and without flux adjustment. *Geophys. Res. Lett.* **24**, 1943–1946 (1997).
50. J. M. Gregory, M. J. F. B, The role of climate sensitivity and ocean heat uptake on AOGCM transient temperature response. *J. Clim.* **15**, 124–130 (2002).
51. J. M. Gregory, T. Andrews, P. Good, The inconstancy of the transient climate response parameter under increasing CO_2. *Philos. Trans. R. Soc. A* **373**, 20140417 (2015).
52. Y. Dong, A. Pauling, S. Sadai, K. C. Armour, Antarctic ice-sheet meltwater reduces transient warming and climate sensitivity through the sea-surface temperature pattern effect. *Geophys. Res. Lett.* **49**, e2022GL101249 (2022).

53. R. P. Allan *et al*., Changes in global net radiative imbalance 1985–2012. *Geophys. Res. Lett.* **41**, 5588–5597 (2014).
54. J. M. Gregory, Vertical heat transports in the ocean and their effect on time-dependent climate change. *Clim. Dyn.* **16**, 501–515 (2000).
55. I. M. Held *et al*., Probing the fast and slow components of global warming by returning abruptly to preindustrial forcing. *J. Clim.* **23**, 2418–2427 (2010).
56. O. Geoffroy *et al*., Transient climate response in a two-layer energy-balance model. Part II: Representation of the efficacy of deep-ocean heat uptake and validation for CMIP5 AOGCMS. *J. Clim.* **26**, 1859–1876 (2013).
57. Y. Dong, K. C. Armour, D. S. Battisti, E. Blanchard-Wrigglesworth, Two-way teleconnections between the Southern Ocean and the Tropical Pacific via a dynamic feedback. *J. Clim.* **35**, 2667–2682 (2022).
58. E. Blanchard-Wrigglesworth, L. A. Roach, A. Donohoe, Q. Ding, Impact of winds and southern ocean SSTS on Antarctic Sea ice trends and variability. *J. Clim.* **34**, 949–965 (2021).
59. A. G. Pauling, C. M. Bitz, I. J. Smith, P. J. Langhorne, The response of the Southern Ocean and Antarctic Sea ice to freshwater from ice shelves in an Earth system model. *J. Clim.* **29**, 1655–1672 (2016).
60. C. J. Smith, P. M. Forster, Suppressed late-20th century warming in cmip6 models explained by forcing and feedbacks. *Geophys. Res. Lett.* **48**, e2021GL094948 (2021).
61. J. T. Fasullo *et al*., Spurious late historical-era warming in CESM2 driven by prescribed biomass burning emissions. *Geophys. Res. Lett.* **49**, e2021GL097420 (2022).
62. A. G. Pauling, C. M. Bitz, K. C. Armour, The climate response to the Mt. Pinatubo eruption does not constrain climate sensitivity. *Geophys. Res. Lett.* **50**, e2023GL102946 (2023).
63. Y. Liang, N. P. Gillett, A. H. Monahan, Climate model projections of 21st century global warming constrained using the observed warming trend. *Geophys. Res. Lett.* **47**, e2019GL086757 (2020).
64. A. Ribes, S. Qasmi, N. P. Gillet, Making climate projections conditional on historical observations. *Sci. Adv.* **7**, eabc0671 (2021).
65. J. Zhu *et al*., Assessment of equilibrium climate sensitivity of the community earth system model version 2 through simulation of the last glacial maximum. *Geophys. Res. Lett.* **48**, e2020GL091220 (2021).
66. T. Laepple, P. Huybers, Global and regional variability in marine surface temperatures. *Geophysi. Res. Lett.* **41**, 2528–2534 (2014).
67. T. Laepple, P. Huybers, Ocean surface temperature variability: Large model-data differences at decadal and longer periods. *Proc. Natl. Acad. Sci. U.S.A.* **111**, 16682–16687 (2014).
68. B. J. Henley *et al*., Spatial and temporal agreement in climate model simulations of the interdecadal pacific oscillation. *Environ. Res. Lett.* **12**, 044011 (2017).
69. S. Po-Chedley *et al*., Natural variability contributes to model-satellite differences in tropical tropospheric warming. *Proc. Natl. Acad. Sci. U.S.A.* **118**, e2020962118 (2021).
70. Y. Kostov, D. Ferreira, K. C. Armour, J. Marshall, Contributions of greenhouse gas forcing and the southern annular mode to historical southern ocean surface temperature trends. *Geophys. Res. Lett.* **45**, 1086–1097 (2018).
71. D. L. Hartmann, The Antarctic ozone hole and the pattern effect on climate sensitivity. *Proc. Natl. Acad. Sci. U.S.A.* **119**, e2207889119 (2022).
72. A. Purich, M. H. England, W. Cai, A. Sullivan, P. J. Durack, Impacts of broad-scale surface freshening of the southern ocean in a coupled climate model. *J. Clim.* **31**, 2613–2632 (2018).
73. C. Takahashi, M. Watanabe, Pacific trade winds accelerated by aerosol forcing over the past two decades. *Nat. Clim. Change* **6**, 768–772 (2016).
74. S. McGregor, M. F. Stuecker, J. B. Kajtar, M. H. England, M. Collins, Model tropical Atlantic biases underpin diminished pacific decadal variability. *Nat. Clim. Change* **8**, 493–498 (2018).
75. T. Kohyama, D. L. Hartmann, D. S. Battisti, La niña–like mean-state response to global warming and potential oceanic roles. *J. Clim.* **30**, 4207–4225 (2017).
76. R. Seager *et al*., Strengthening tropical pacific zonal sea surface temperature gradient consistent with rising greenhouse gases. *Nat. Clim. Change* **9**, 517–522 (2019).
77. T. Rackow *et al*., Delayed Antarctic sea-ice decline in high-resolution climate change simulations. *Nat. Commun.* **13**, 637 (2023).
78. A. D. Haugstad, K. C. Armour, D. S. Battisti, B. E. J. Rose, Relative roles of surface temperature and climate forcing patterns in the inconstancy of radiative feedbacks. *Geophys. Res. Lett.* **44**, 7455–7463 (2017).
79. M. Zhou *et al*., Explaining forcing efficacy with pattern effect and state dependence. *Geophys. Res. Lett.* **50**, e2022GL101700 (2023).
80. H. Kim, S. M. Kang, J. E. Kay, S. P. Xie, Subtropical clouds key to southern ocean teleconnections to the tropical pacific. *Proc. Natl. Acad. Sci. U.S.A.* **119**, e2200514119 (2022).
81. W. R. Frey, E. A. Maroon, A. G. Pendergrass, J. E. Kay, Do southern ocean cloud feedbacks matter for 21st century warming? *Geophys. Res. Lett.* **11**, 33–37 (2017).
82. M. Watanabe, J. L. Dufresne, Y. Kosaka, T. Mauritsen, T. Hiroaki, Enhanced warming constrained by past trends in equatorial Pacific Sea surface temperature gradient. *Nat. Clim. Change* **11**, 33–37 (2021).
83. A. Gjermundsen *et al*., Shutdown of southern ocean convection controls long-term greenhouse gas-induced warming. *Nat. Geosci.* **14**, 724–731 (2021).
84. J. E. Tierney, A. M. Haywood, R. Fend, T. Bhattacharya, B. L. Otto-Bliesner, Pliocene warmth consistent with greenhouse gas forcing. *Geophys. Res. Lett.* **46**, 9136–9144 (2019).
85. N. J. Lutsko, M. Popp, Probing the sources of uncertainty in transient warming on different timescales. *Geophys. Res. Lett.* **46**, 11367–11377 (2019).
86. K. C. Armour, Data from: Sea-surface temperature pattern effects have slowed global warming and biased warming-based constraints on climate sensitivity. Dryad. https://doi.org/10.5061/dryad.zgmsbcckd. Deposited 29 January 2023.